


Contraction velocity of viscoelastic filaments

Xiao Liu , Brayden W. Wagoner,^{*} and Osman A. Basaran [†]*Davidson School of Chemical Engineering, Purdue University, 480 Stadium Mall Drive, West Lafayette, Indiana 47907, USA*

(Received 3 August 2022; accepted 7 December 2022; published 26 December 2022; corrected 24 January 2023)

Liquid filaments, which are commonplace in daily life, nature, and technology, including inkjet printing and crop spraying, contract due to surface tension: they either retract into a single sphere or break up to produce a primary drop(s) and several smaller satellites. The latter are undesirable because they reduce printing quality and cause pollution due to spray drift. Surfactants and/or polymer additives can be used to control filament contraction and breakup. It has recently been demonstrated experimentally that the velocity at which the tips of contracting filaments retract can be increased in viscoelastic filaments that contain polymer additives compared to purely Newtonian filaments. Here, simulations are used to investigate the contraction of viscoelastic filaments whose rheology is described by the Oldroyd-B model. Filaments produced from nozzles are expected to be prestressed when they begin to contract. It is shown that the velocity with which the tips of prestressed filaments retract is greatly increased compared to filaments in which the polymer molecules are relaxed. This enhancement is explained by examining the value of $\boldsymbol{\sigma} : \mathbf{D}$ ($\boldsymbol{\sigma}$: Elastic stress; \mathbf{D} : Rate-of-strain tensor), which can be positive or negative. This quantity is positive when the flow does work on the polymer molecules but negative when the molecules do work on the flow, i.e., when elastic recoiling or unloading takes place. In prestressed filaments, elastic unloading takes place because $\boldsymbol{\sigma} : \mathbf{D} < 0$: The elastic stresses work by pulling the fluid in axially and pushing it out radially, thereby drastically increasing the tip velocity.

DOI: [10.1103/PhysRevFluids.7.L121601](https://doi.org/10.1103/PhysRevFluids.7.L121601)

Introduction. Filaments consist of slender, cylindrical central sections that are capped by two bulbous ends and are ubiquitous in applications including inkjet printing [1–7] and atomization, e.g., spray coating and crop spraying [8–11]. Driven by the capillary pressure difference between their bulbous caps and main cylindrical bodies, filaments contract. During contraction, they either contract into spheres or disintegrate, as they retract, into one or more primary drops and multiple smaller satellite droplets [1,12–17]. The satellites are undesirable in applications because they reduce printing quality [1,2,18] and lead to spray drift [10,11,19]. The interplay between inertia and capillary and viscous stresses determines the dynamics and different breakup modes that result when the filaments are Newtonian fluids [16].

In applications, the working liquids often contain surfactant [6,20] and/or polymer additives [2,18]. These serve numerous purposes, including controlling breakup. Polymer addition to the Newtonian solvent gives rise to viscoelastic stresses [21] which, along with inertia, capillary pressure, and viscous stresses, control the dynamics of filament contraction. While there exist extensive studies on the stability of viscoelastic jets [22–35], most of these works focus on capillary

^{*}Now at 3M, St. Paul, Minnesota, USA

[†]obasaran@purdue.edu

thinning of jets and bridges. Filaments, however, exhibit retraction of bulbous ends in addition to thinning and breakup. Therefore, of great relevance to filament contraction are the pioneering studies [36,37] that showed that a circular hole in an inviscid planar liquid sheet grows at a constant value, viz., the Taylor-Culick velocity. Indeed, the retraction velocity of tips of Newtonian filaments/sheets has attracted much theoretical attention (see, e.g., Ref. [38]) and has been a source of experimental controversy [14,39]. Despite its importance in applications, the retraction velocity of viscoelastic filaments has only received scant attention. Only quite recently, Sen *et al.* [18] have shown through a combination of experiments and a control volume argument that highly stretched dumbbell-shaped viscoelastic filaments retract at velocities that exceed the Newtonian Taylor-Culick velocity. The goal of this work is to use simulation to advance the understanding of the retraction velocity of viscoelastic filaments whose rheology is described by the Oldroyd-B model [21]. In particular, we account here for the fact that when fluid is emitted from nozzles, highly stretched filaments are produced within which polymer molecules are prestressed rather than relaxed as they begin to contract, as discussed in Sen *et al.* [18].

The remainder of the paper is organized as follows. We first present the mathematical formulation of the problem. Here, we take advantage of filament slenderness and analyze the contraction dynamics by using the slender-jet equations. Next, we demonstrate that the contraction velocity of viscoelastic filaments can be substantially increased if polymer molecules are prestressed initially and that polymers with larger relaxation times lead to larger increases in contraction velocity. The reason behind the drastic increase in contraction velocity of viscoelastic filaments is then probed by analyzing the time evolution of the underlying forces. We then demonstrate that the enhancement of contraction velocity can be rationalized by quantifying elastic recoil within contracting viscoelastic filaments.

Mathematical formulation and numerical method. The system is isothermal and consists of an axisymmetric liquid filament that contains dissolved polymer molecules, and is surrounded by a dynamically passive gas that exerts a constant pressure on the filament. The surface tension γ of the interface is also constant. The polymer solution is incompressible and has uniform composition with constant density ρ_s , solvent viscosity μ_s , and polymer viscosity μ_p . The relaxation time of the polymer is denoted by $\tilde{\lambda}$.

It proves convenient to use a cylindrical coordinate system $(\tilde{r}, \theta, \tilde{z})$ with its origin at the intersection of the line of axisymmetry and midplane of symmetry [Fig. 1(a)]. Thus, the \tilde{z} coordinate runs along the symmetry axis, the radial coordinate \tilde{r} is the distance from that axis, and θ is the usual angle measured around that axis. As a result of these inherent symmetries, the problem domain is a single quadrant of the (\tilde{r}, \tilde{z}) plane [Fig. 1(b)].

We next nondimensionalize the problem using initial filament radius as characteristic length, $l_c \equiv R$, and inertial-capillary time as characteristic time, $t_c \equiv \sqrt{\rho R^3/\gamma}$. Furthermore, we use the ratio of these two scales as characteristic velocity $v_c \equiv l_c/t_c = \sqrt{\gamma/\rho R}$, which is the Taylor-Culick velocity \tilde{v}_{TC} . The capillary pressure is adopted as characteristic pressure, $p_c \equiv \gamma/R$, and the characteristic stress scale is taken to be $\sigma_c \equiv \mu_s/t_c$. As a result, the problem is governed by four dimensionless groups: Ohnesorge number $\text{Oh} \equiv \mu_s/\sqrt{\rho R \gamma}$, Deborah number $\text{De} \equiv \tilde{\lambda}/t_c$, ratio of polymer to Newtonian solvent viscosity $\beta \equiv \mu_p/\mu_s$, and dimensionless initial aspect ratio $L_0 = \tilde{L}_0/R$ (\tilde{L}_0 : initial filament half-length). Dimensionless groups other than those used here are also common. In lieu of Oh and β , Fontelos and Li [40] have used two Ohnesorge numbers, one based on the solvent viscosity and the other on the polymer viscosity. Alternatively, the total viscosity, $\mu_0 = \mu_s + \mu_p$, can be used to define an Ohnesorge number as $\text{Oh}_{\text{alt}} \equiv \mu_0/\sqrt{\rho R \gamma}$ and the ratio of solvent to total viscosity can be used to define a viscosity ratio as $\beta_{\text{alt}} \equiv \mu_s/\mu_0$. The latter set and that used here are related as $\text{Oh}_{\text{alt}} = \text{Oh}(1 + \beta)$ and $\beta_{\text{alt}} = 1/(1 + \beta)$. Hereafter, variables without tildes are the dimensionless counterparts of those with tildes, e.g., \tilde{t} is dimensional but $t \equiv \tilde{t}/t_c$ is dimensionless.

The dynamics of viscoelastic filament contraction is governed by the three-dimensional but axisymmetric (3DA) continuity and Cauchy momentum equations *and* the traction and kinematic boundary conditions at the free surface [31,41]. In lieu of solving a complex 3DA free surface

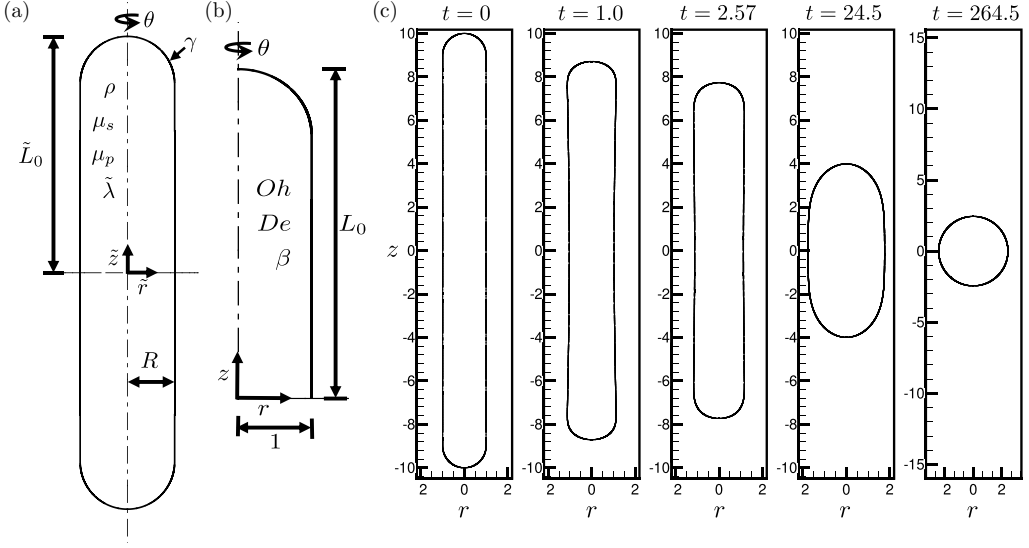


FIG. 1. Viscoelastic filament: (a) Definition sketch and (b) problem domain. (c) Evolution in time of the shape of a prestressed viscoelastic filament of $Oh = 5$, $L_0 = 10$, $De = 0.1$, $\beta = 0.25$, and $\sigma_{zz,0} = 10$.

flow [42], we take advantage of filament slenderness and adopt the slender-jet formalism that was originally developed for Newtonian fluids in Refs. [43,44] and which was subsequently extended to viscoelastic fluids [30,45]. Thus, we solve the following one-dimensional (1D) transient evolution equations to determine the interface shape $r = h(z, t)$ (h : interface shape function) and axial velocity $v = v(z, t)$:

$$\frac{\partial v}{\partial t} + v \frac{\partial v}{\partial z} = \frac{\partial}{\partial z}(-2\mathcal{H}) + 3Oh \frac{1}{h^2} \frac{\partial}{\partial z} \left(h^2 \frac{\partial v}{\partial z} \right) + Oh \frac{1}{h^2} \frac{\partial}{\partial z} [h^2(\sigma_{zz} - \sigma_{rr})], \quad (1)$$

$$\frac{\partial h}{\partial t} + v \frac{\partial h}{\partial z} + \frac{1}{2} \frac{\partial v}{\partial z} h = 0, \quad (2)$$

where $-2\mathcal{H}$ is twice the mean curvature and σ_{rr} and σ_{zz} are the radial and axial components of the elastic stress tensor σ . Following earlier works [43,44,46,47], we retain the complete expression for the mean curvature such that $2\mathcal{H} = (1/h)[1 + (\partial h/\partial z)^2]^{-1/2} - (\partial^2 h/\partial z^2)[1 + (\partial h/\partial z)^2]^{-3/2}$. The radial and axial components of the elastic stress tensor σ_{rr} and σ_{zz} for the Oldroyd-B fluid in Eq. (1) are governed by the following evolution equations:

$$\frac{\partial \sigma_{rr}}{\partial t} + v \frac{\partial \sigma_{rr}}{\partial z} = -\sigma_{rr} \frac{\partial v}{\partial z} - \frac{\beta}{De} \frac{\partial v}{\partial z} - \frac{1}{De} \sigma_{rr}, \quad (3)$$

$$\frac{\partial \sigma_{zz}}{\partial t} + v \frac{\partial \sigma_{zz}}{\partial z} = 2\sigma_{zz} \frac{\partial v}{\partial z} + 2 \frac{\beta}{De} \frac{\partial v}{\partial z} - \frac{1}{De} \sigma_{zz} \quad (4)$$

The set of equations are solved subject to the boundary conditions that at the plane of symmetry ($z = 0$), $\partial h/\partial z = 0$ and $v = 0$. At the filament tip, $h = 0$ and $v = dL/dt$, where $L(t)$ is the instantaneous but unknown half-length of the filament or location of the filament tip [47]. The tip location, $z = L(t)$, is determined by an integral constraint that filament volume is fixed [47].

Furthermore, we allow for the possibility that at $t = 0$, polymer molecules within the filament may be prestressed such that the axial component of the elastic stress tensor σ_{zz} equals some positive constant, viz., $\sigma_{zz}(z, t = 0) = \sigma_{zz,0}$, which is the simplest functional form that can be adopted

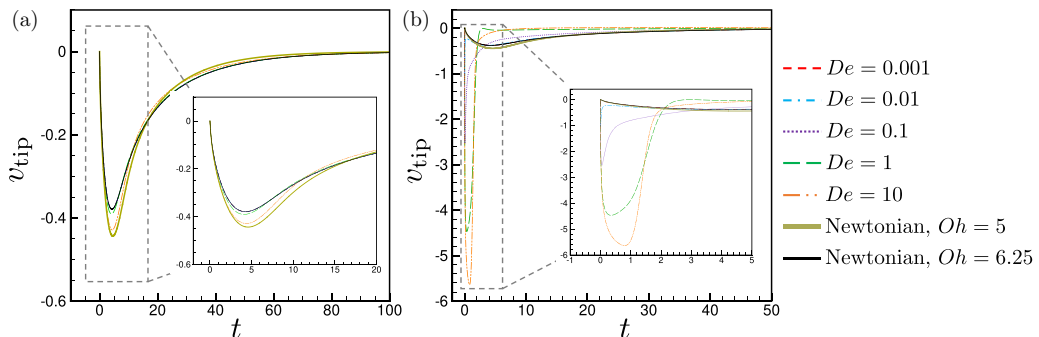


FIG. 2. Variation of tip velocity v_{tip} with time t during contraction of viscoelastic and Newtonian filaments of $L_0 = 10$. For viscoelastic filaments, $\text{Oh} = 5$ and $\beta = 0.25$: (a) $\sigma_{zz,0} = 0$ (polymer molecules are initially relaxed) and (b) $\sigma_{zz,0} = 10$ (polymer molecules are initially prestressed). The curves corresponding to the different viscoelastic filaments are identified by both color and line type as: (red dash) $De = 0.001$, (blue dash dot) $De = 0.01$, (purple dotted) $De = 0.1$, (green long dash) $De = 1$, and (orange dash dot dot) $De = 10$. The olive thick solid curve and black thin solid curve correspond to Newtonian filaments of $\text{Oh} = 5$ and $\text{Oh} = 6.25$, respectively. In (a), the curves depicting the time evolution of v_{tip} corresponding to viscoelastic filaments of $De = 0.001, 0.01$, and 0.1 are virtually indistinguishable from that of the Newtonian filament of $\text{Oh} = 6.25$.

to approximate and gain insights into the role of initially unrelaxed viscoelastic stresses on the contraction dynamics. Based on the the work of Sen *et al.* [18], who have observed that $\sigma_{zz,0}$ is in the range of $\mathcal{O}(10)$ – $\mathcal{O}(100)$ in their experiments, we report below simulation results when $\sigma_{zz,0} = 10$.

Equations (1)–(4) are solved by the method of lines using the Galerkin/finite element method [47].

Results and discussion: Contraction velocity. In the remainder of the article, we consider the dynamics of highly viscous filaments ($\text{Oh} > 1$) of small initial aspect ratios ($L_0 = 10$) that eventually contract to spheres. We note that our filaments are both shorter and much more viscous than those studied in Sen *et al.* [18], where $\text{Oh} = \mathcal{O}(0.01)$. We focus on (i) viscous filaments to avoid more complex dynamics involving capillary waves that arise with low Oh filaments and (ii) small aspect ratios to preclude breakup [13,16]. One characteristic feature of the dynamics when Oh is large is the uniform thickening of the contracting filament in time, which is analogous to the response of retracting films reported in Refs. [48,49]. Figure 1(c) shows the evolution in time of the shape of a prestressed viscoelastic filament. As time increases, the filament length continuously shortens but the two ends remain virtually hemispherical without the formation of bulbous tips that arise during contraction of filaments of intermediate or low viscosity [16].

Figure 2(a) shows the variation in time of the tip velocity v_{tip} of several highly viscous filaments of identical initial aspect ratio. Five of these are viscoelastic filaments that are initially relaxed ($\sigma_{zz,0} = 0$) and all of $\text{Oh} = 5$ and $\beta = 0.25$ but various De , and two are Newtonian filaments of $\text{Oh} = 5$ and $\text{Oh} = 6.25$. The two Newtonian filaments are such that $\text{Oh}_{\text{Newtonian}} = \text{Oh}_{\text{viscoelastic}}$ in one case and $\text{Oh}_{\text{Newtonian}} = (1 + \beta)\text{Oh}_{\text{viscoelastic}}$ in the second case. According to Fig. 2(a), when polymer molecules are initially at equilibrium, the contraction velocity of viscoelastic filaments is invariant with respect to De when $0.001 \leq De \leq 0.1$. Moreover, the dynamical response in all of the just-stated three cases is virtually identical to that of the Newtonian filament of $\text{Oh} = 6.25$. As De increases, the magnitude of the peak contraction velocity increases compared to these four cases. According to Fig. 2(a), the Newtonian filament of $\text{Oh} = 5$ attains the contraction velocity with the largest peak magnitude. Clearly, as shown in Fig. 2(a), the overall difference between v_{tip} of viscoelastic filaments and Newtonian ones is small when polymer molecules are initially at equilibrium. It is worth noting that the magnitudes of the peak values of the contraction velocity of Newtonian filaments are smaller than the Taylor-Culick velocity v_{TC} in Fig. 2(a). This observation is in accord with [50] where it was shown that highly viscous filaments contract in a transient regime

of long duration before $v_{\text{tip}} \approx v_{\text{TC}}$ and the tips of such filaments do not attain v_{TC} prior to full recoil if their L_0 are sufficiently small.

Figure 2(b) shows the variation in time of v_{tip} of filaments that have identical values of the dimensionless parameters as those in Fig. 2(a) except that the five viscoelastic filaments in Fig. 2(b) are now initially prestressed ($\sigma_{zz,0} = 10$). Figure 2(b) shows that the contraction velocities of prestressed viscoelastic filaments of $\text{De} \geq 0.1$ are several times as large as those of filaments for which $\sigma_{zz,0} = 0$. For example, the peak contraction velocity of a prestressed viscoelastic filament when $\text{De} = 10$ is ten times that of a viscoelastic filament that has not been prestressed or that of either Newtonian filament. This finding agrees with experimental observations reported in Ref. [18] that viscoelastic retraction is faster than Newtonian retraction. However, comparison of the results reported in Figs. 2(a) and 2(b) makes clear that it is only when polymer molecules are prestressed that a large increase in contraction velocity results. According to Fig. 2(b), prestressed viscoelastic filaments exhibit much larger differences in dynamical response during the initial stages in which the filament tips undergo acceleration compared to viscoelastic filaments in which the polymer molecules are initially at equilibrium. Moreover, when $\sigma_{zz,0} \neq 0$, the larger De is, the larger the peak magnitude of contraction velocity and the longer the duration over which the spike in v_{tip} can be observed [inset to Fig. 2(b)]. The difference in the magnitude of the peak velocity attained when molecules are prestressed versus when they are initially relaxed is drastic: For example, when $\text{De} = 10$, the peak magnitude of the contraction velocity is larger than 5 in the former case, whereas it is about 0.4 in the latter. The reasons behind this stark difference are discussed next.

Force balance. One way to elucidate the interplay between inertia and capillary, viscous, and elastic forces during filament contraction is by performing an integral force balance [18,39,50–52]. Here, we adopt the approach presented in Ref. [39] to carry out such an analysis. By rewriting the momentum equation [Eq. (1)] as

$$\frac{\partial v}{\partial t} + v \frac{\partial v}{\partial z} = \frac{1}{h^2} \frac{\partial}{\partial z} (h^2 K) + 3\text{Oh} \frac{1}{h^2} \frac{\partial}{\partial z} \left(h^2 \frac{\partial v}{\partial z} \right) + \text{Oh} \frac{1}{h^2} \frac{\partial}{\partial z} [h^2 (\sigma_{zz} - \sigma_{rr})], \quad (5)$$

where $K = (1/h)[1 + (\partial h/\partial z)^2]^{-1/2} + (\partial^2 h/\partial z^2)[1 + (\partial h/\partial z)^2]^{-3/2}$, the two equations governing momentum and mass conservation [Eq. (2)] are combined by first multiplying Eq. (5) by h^2 and then adding the result to Eq. (2) multiplied by $2hv$. The resulting expression is then integrated with respect to z from 0 (filament's midplane) to $L(t)$ (filament's tip) and simplified by taking advantage of the boundary conditions at the two locations to yield

$$\underbrace{\frac{dP_{\text{tot}}}{dt}}_{\text{inertia}} = \underbrace{\left[-h^2 \left(\frac{\partial^2 h}{\partial z^2} + \frac{1}{h} \right) \right]_{z=0}}_{\text{capillary}} + \underbrace{\left(-3\text{Oh} h^2 \frac{\partial v}{\partial z} \right)_{z=0}}_{\text{viscous}} + \underbrace{[-\text{Oh} h^2 (\sigma_{zz} - \sigma_{rr})]_{z=0}}_{\text{elastic}}, \quad (6)$$

where $P_{\text{tot}} = \int_0^{L(t)} h^2 v dz$. In Eq. (6), πP_{tot} is the total momentum of the fluid occupying one-half of the filament volume between $0 \leq z \leq L(t)$, and the time rate of change of momentum (the inertia term on the left side) equals the sum of the capillary, viscous, and elastic forces (the three terms on the right side).

Figure 3 shows the variation in time of the terms in Eq. (6) in four situations. In Fig. 3(a), the time evolution of the three terms— inertia and capillary and viscous forces—is shown for a Newtonian filament of $\text{Oh} = 6.25$. In Figs. 3(b)–3(d), the time evolution of the four terms— inertia and capillary, viscous, and elastic forces—is shown for three viscoelastic filaments: a large De filament in which the molecules are initially at equilibrium ($\sigma_{zz,0} = 0$), and two filaments, one of $\text{De} = 0.1$ and the other of $\text{De} = 10$, that are initially prestressed ($\sigma_{zz,0} = 10$). Figures 3(a) and 3(b) show that for the Newtonian filament and the filament in which polymer molecules are initially at equilibrium, inertia is small compared to the capillary and viscous forces during most of the contraction process. While the forces vary temporally, capillary and viscous forces are comparable and typically are about 10 to 100 times as large as inertia. The order of magnitude difference between viscous/capillary forces and inertia is expected because Oh is high ($\text{Oh} = 6.25$ and 5). In Fig. 3(b),

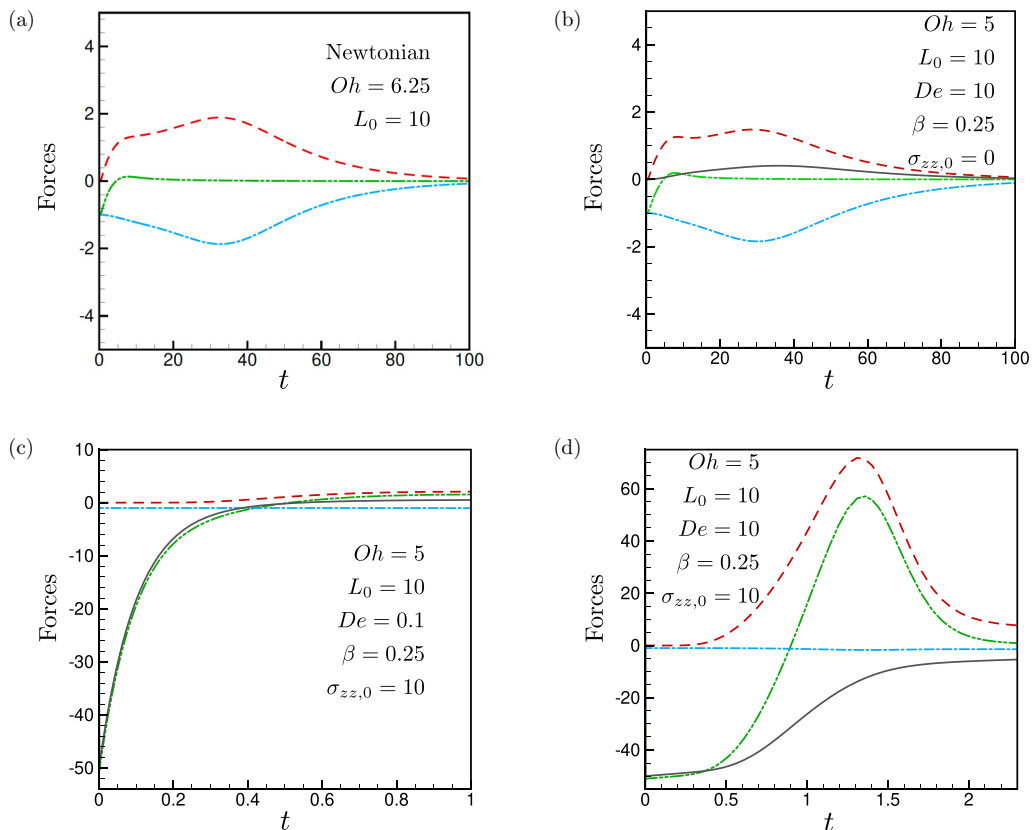


FIG. 3. Variation with time t of the various forces obtained from Eq. (6) during contraction of filaments of $L_0 = 10$. (a) Newtonian filament of $Oh = 6.25$. (b) Viscoelastic filament of $Oh = 5$, $De = 10$, $\beta = 0.25$, and $\sigma_{zz,0} = 0$ (polymer molecules are initially relaxed). (c) Prestressed viscoelastic filament of $Oh = 5$, $De = 0.1$, $\beta = 0.25$, and $\sigma_{zz,0} = 10$. (d) Prestressed viscoelastic filament of $Oh = 5$, $De = 10$, $\beta = 0.25$, and $\sigma_{zz,0} = 10$. The curves corresponding to the different terms in Eq. (6) are identified by both color and line type as: (green dash dot dot) inertia, (blue dash dot) capillary force, (red dashed) viscous force, and (dark gray solid) elastic force.

elastic stresses are also negligible compared to viscous and capillary stresses, leading to similar contraction dynamics as shown by the black and orange curves in Fig. 2(a).

However, if polymer molecules are prestressed, the dynamical response of highly viscous viscoelastic filaments resembles the trend observed in the responses of low- Oh filaments since inertia comes into play. When $De = 0.1$, inertia and elastic force are comparable and capillary and viscous forces are negligible, as shown in Fig. 3(c) when $t \leq 0.2$. In the case of higher $De = 10$, elastic force takes longer to decrease and reach a plateau compared to the case of lower $De = 0.1$. In the former case, significant viscous stresses also develop to balance the larger inertia as shown at $t \approx 1.3$ in Fig. 3(d). Comparing Figs. 3(c) and 3(d) reveals that elastic stresses take more time to decay with increasing Deborah number, in agreement with the strong dependence of the evolution of v_{tip} with De shown in Fig. 2(b). In summary, while for Newtonian and nonprestressed viscoelastic filaments the retraction is driven by capillarity and resisted by viscosity, for sufficiently prestressed viscoelastic filaments, the driving retraction force is viscoelasticity, which is now resisted by inertia and viscosity, with negligible capillary effects.

Elastic recoil. The increase in contraction velocity of prestressed viscoelastic filaments may be rationalized by the fact that polymer molecules pull fluid as they recoil from a prestressed state to the

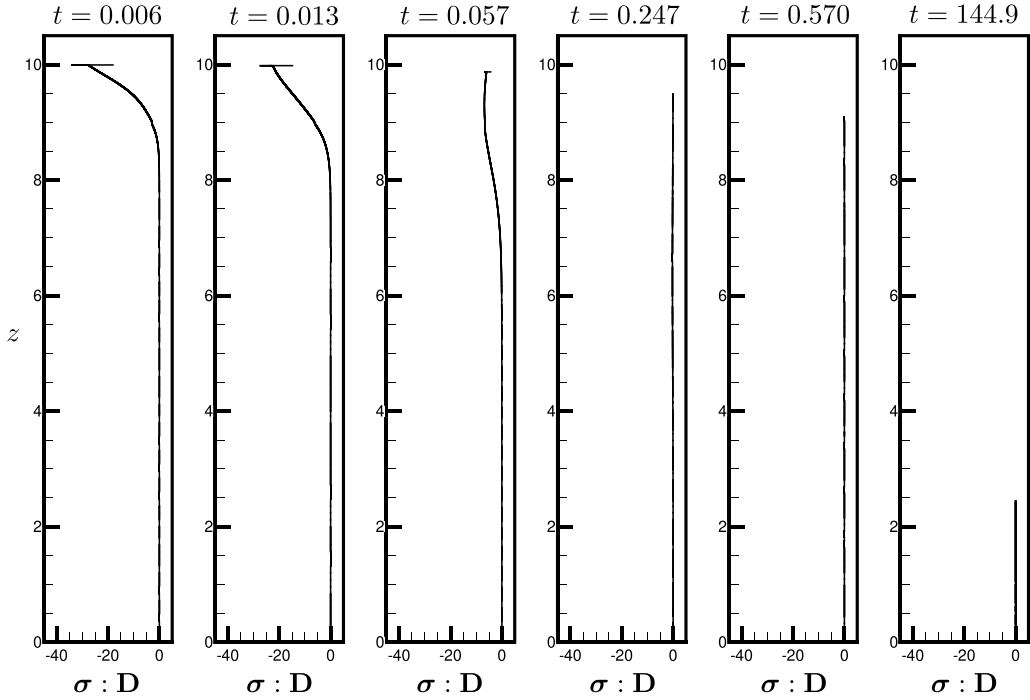


FIG. 4. Elastic recoil in a prestressed viscoelastic filament of small De : Evolution in time of $\boldsymbol{\sigma} : \mathbf{D}$ when $Oh = 5$, $L_0 = 10$, $De = 0.1$, $\beta = 0.25$, and $\sigma_{zz,0} = 10$.

equilibrium state. This action can be probed by evaluating the amount of elastic unloading or recoil that takes place near the filament's tip(s). Following the explanation provided in Ref. [31], we first note that the expression for the conversion of mechanical energy into internal energy is $\mathbf{T} : \nabla \mathbf{v} = \mathbf{T} : \mathbf{D} = (\boldsymbol{\tau} + \boldsymbol{\sigma}) : \mathbf{D}$, where \mathbf{T} , $\boldsymbol{\tau}$, and \mathbf{D} denote the total stress, viscous stress, and rate-of-strain tensors. Whereas viscous dissipation $\boldsymbol{\tau} : \mathbf{D}$ is always positive, $\boldsymbol{\sigma} : \mathbf{D}$ can be positive or negative. This quantity is positive when the flow does work on the polymer molecules but negative when the molecules do work on the flow. Thus, elastic unloading takes place in the filament wherever $\boldsymbol{\sigma} : \mathbf{D}$ is negative. Physically, when $\boldsymbol{\sigma} : \mathbf{D} < 0$, elastic stresses work by pulling the fluid in axially and pushing it out radially as molecules recoil from a stretched state. In slender-jet analysis, $\boldsymbol{\sigma} : \mathbf{D} = (\sigma_{zz} - \sigma_{rr}) \frac{\partial v}{\partial z} + \mathcal{O}(r^2)$.

Figure 4 shows the evolution in time of $\boldsymbol{\sigma} : \mathbf{D}$ of a prestressed viscoelastic filament of small De ($= 0.1$). At early times, $\boldsymbol{\sigma} : \mathbf{D} < 0$ in the tip region, but its magnitude gradually decreases as the filament contracts. Therefore, even though the contraction process is accelerated as polymer molecules do work on the flow by pulling fluid in axially, this effect fades quickly as polymer molecules recover from their stretched state and tend to equilibrium. At $t = 0.247$, $\boldsymbol{\sigma} : \mathbf{D} \approx 0$ in the entire domain, which implies that polymer molecules are no longer acting in an appreciable way on the flow by pulling the fluid in axially. Thereafter, the contraction is driven solely by the capillary pressure difference between the the filament's tips and its cylindrical body, as is the case with Newtonian filaments.

Figure 5 shows the evolution in time of $\boldsymbol{\sigma} : \mathbf{D}$ of a prestressed viscoelastic filament of the same set of parameters as the one shown in Fig. 4 but with a higher Deborah number ($De = 10$). While the overall evolution in time of $\boldsymbol{\sigma} : \mathbf{D}$ is similar in both cases, i.e., $\boldsymbol{\sigma} : \mathbf{D} < 0$, and its magnitude decreases in time, $\boldsymbol{\sigma} : \mathbf{D}$ remains nonzero and negative for a longer time for the filament of higher De (longer relaxation time). For instance, around $t = 0.56$, $\boldsymbol{\sigma} : \mathbf{D} = 0$ when $De = 0.1$ in Fig. 4 but $\boldsymbol{\sigma} : \mathbf{D} < 0$ when $De = 10$ in Fig. 5. This longer duration over which $\boldsymbol{\sigma} : \mathbf{D} < 0$ when $De = 10$

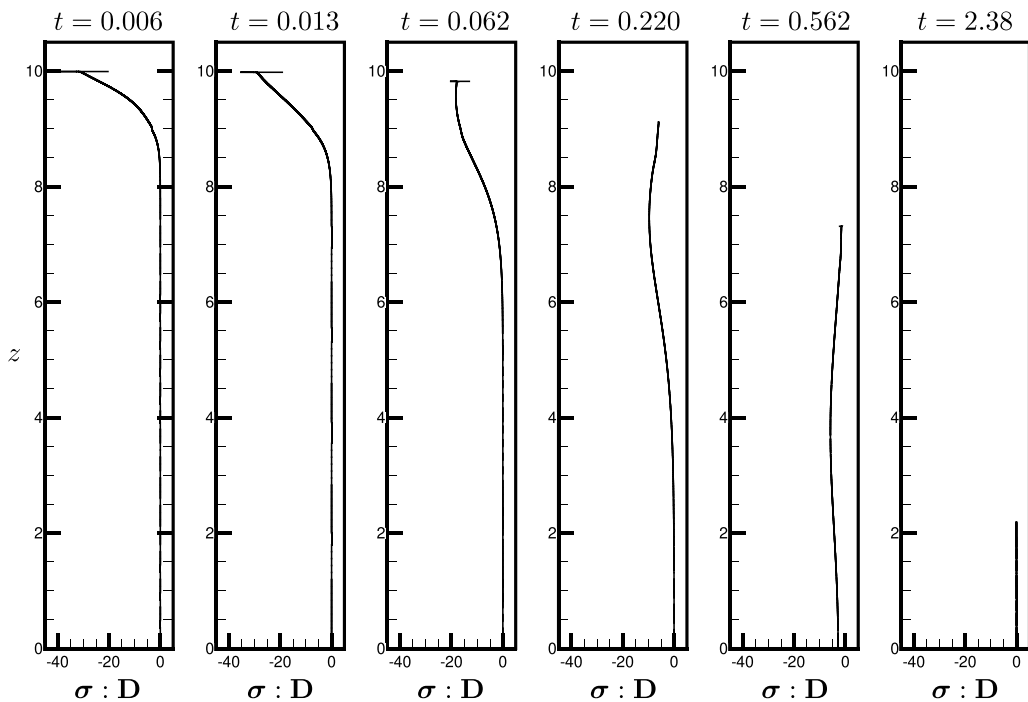


FIG. 5. Elastic recoil in a prestressed viscoelastic filament of large De : Evolution in time of $\sigma : \mathbf{D}$ when $Oh = 5$, $L_0 = 10$, $De = 10$, $\beta = 0.25$, and $\sigma_{zz,0} = 10$.

compared to when $De = 0.1$ accounts for the larger and wider spike in contraction velocity in the former case compared to the latter one, as shown by the orange and the purple curves in Fig. 2(b).

It is instructive to examine the results of Figs. 4 and 5 in terms of time made dimensionless with the relaxation time of the polymer: $t^* \equiv \tilde{t}/\tilde{\lambda} = (\tilde{t}/t_c)(t_c/\tilde{\lambda}) \equiv t/De$. It is shown in Fig. 4 that for $De = 0.1$, the prestressed polymer molecules in the contracting viscoelastic filament are relaxed when $t \approx 0.24$, but it is shown in Fig. 5 that for $De = 10$, the time for the molecules to relax is $t \approx 2.4$. If these dimensionless times for relaxation of polymer molecules were recast into times made dimensionless by $\tilde{\lambda}$, $t^* \approx 0.24/0.1 = 2.4$ when $De = 0.1$ and $t^* \approx 2.4/10 = 0.24$ when $De = 10$. Therefore, the prestresses have not relaxed at roughly the same value of $t^* = \tilde{t}/\tilde{\lambda}$ in the two cases.

Conclusions. According to the foregoing results, contraction velocity v_{tip} of prestressed viscoelastic filaments ($\sigma_{zz,0} \neq 0$) in which polymer molecules are highly extended at the onset of retraction can be many times larger than ones in which polymer molecules are initially in a relaxed state or Newtonian filaments of the same Oh . This finding, which has important ramifications in applications with respect to formation of satellite droplets [1,2,4,6] and accords with recent experiments [18], has been rationalized by examination of $\sigma : \mathbf{D}$, which is a quantity that is analogous to viscous dissipation $\tau : \mathbf{D}$, within the filaments. However, whereas the latter quantity is always positive, the former can be positive or negative. In prestressed viscoelastic filaments, $\sigma : \mathbf{D}$ can be highly negative for a substantial portion of time following the onset of contraction, during which time polymer molecules pull fluid in axially and push it out radially, thereby greatly enhancing v_{tip} . It has also been demonstrated that the duration of this elastic unloading (recoil) can be made longer if a polymer with a higher De (relaxation time) is used.

As Oh and L_0 in this work have been fixed at five and ten, future work should address a wider range of these parameters. The analyses of this article can also be generalized to account for more complex initial conditions (ICs), including nonuniform initial stress profiles as well as asymmetry

in filament shapes [53,54], and consider ICs where the filament fluid is already moving rather than quiescent [39] to better mimic conditions in some experiments [14].

Acknowledgment. We gratefully acknowledge financial support from the Purdue Process Safety and Assurance Center (P2SAC).

-
- [1] O. A. Basaran, Small-scale free surface flows with breakup: Drop formation and emerging applications, *AIChe J.* **48**, 1842 (2002).
 - [2] O. A. Basaran, H. Gao, and P. P. Bhat, Nonstandard inkjets, *Annu. Rev. Fluid Mech.* **45**, 85 (2013).
 - [3] H. Wijshoff, The dynamics of the piezo inkjet printhead operation, *Phys. Rep.* **491**, 77 (2010).
 - [4] J. R. Castrejón-Pita, W. R. S. Baxter, J. Morgan, S. Temple, G. D. Martin, and I. M. Hutchings, Future, opportunities and challenges of inkjet technologies, *Atomiz. Spr.* **23**, 541 (2013).
 - [5] S. D. Hoath, S. Jung, and I. M. Hutchings, A simple criterion for filament break-up in drop-on-demand inkjet printing, *Phys. Fluids* **25**, 021701 (2013).
 - [6] D. Lohse, Fundamental fluid dynamics challenges in inkjet printing, *Annu. Rev. Fluid Mech.* **54**, 349 (2022).
 - [7] A. A. Castrejón-Pita, E. S. Betton, N. Campbell, N. Jackson, J. Morgan, T. R. Tuladhar, D. C. Vadillo, and J. R. Castrejón-Pita, Formulation, quality, cleaning, and other advances in inkjet printing, *Atomiz. Spr.* **31**, 57 (2021).
 - [8] J. Eggers and E. Villermaux, Physics of liquid jets, *Rep. Prog. Phys.* **71**, 036601 (2008).
 - [9] M. Majumder, C. Rendall, M. Li, N. Behabtu, J. A. Eukel, R. H. Hauge, H. K. Schmidt, and M. Pasquali, Insights into the physics of spray coating of SWNT films, *Chem. Eng. Sci.* **65**, 2000 (2010).
 - [10] S. Kooij, R. Sijs, M. M. Denn, E. Villermaux, and D. Bonn, What Determines the Drop Size in Sprays? *Phys. Rev. X* **8**, 031019 (2018).
 - [11] A. Gaillard, R. Sijs, and D. Bonn, What determines the drop size in sprays of polymer solutions? *J. Non-Newtonian Fluid Mech.* **305**, 104813 (2022).
 - [12] H. Stone, B. J. Bentley, and L. G. Leal, An experimental study of transient effects in the breakup of viscous drops, *J. Fluid Mech.* **173**, 131 (1986).
 - [13] P. K. Notz and O. A. Basaran, Dynamics and breakup of a contracting liquid filament, *J. Fluid Mech.* **512**, 223 (2004).
 - [14] A. A. Castrejón-Pita, J. R. Castrejón-Pita, and I. M. Hutchings, Breakup of Liquid Filaments, *Phys. Rev. Lett.* **108**, 074506 (2012).
 - [15] T. Driessen, R. Jeurissen, H. Wijshoff, F. Toschi, and D. Lohse, Stability of viscous long liquid filaments, *Phys. Fluids* **25**, 062109 (2013).
 - [16] C. R. Anthony, P. M. Kamat, M. T. Harris, and O. A. Basaran, Dynamics of contracting filaments, *Phys. Rev. Fluids* **4**, 093601 (2019).
 - [17] F. Wang, F. P. Contò, N. Naz, J. R. Castrejón-Pita, A. A. Castrejón-Pita, C. G. Bailey, W. Wang, J. J. Feng, and Y. Sui, A fate-alternating transitional regime in contracting liquid filaments, *J. Fluid Mech.* **860**, 640 (2019).
 - [18] U. Sen, C. Datt, T. Segers, H. Wijshoff, J. H. Snoeijer, M. Versluis, and D. Lohse, The retraction of jetted slender viscoelastic liquid filaments, *J. Fluid Mech.* **929**, A25 (2021).
 - [19] E. Hilz and A. W. Vermeer, Spray drift review: The extent to which a formulation can contribute to spray drift reduction, *Crop Protection* **44**, 75 (2013).
 - [20] P. M. Kamat, B. W. Wagoner, A. A. Castrejón-Pita, J. R. Castrejón-Pita, C. R. Anthony, and O. A. Basaran, Surfactant-driven escape from endpinching during contraction of nearly inviscid filaments, *J. Fluid Mech.* **899**, A28 (2020).
 - [21] R. B. Bird, R. C. Armstrong, and O. Hassager, *Dynamics of Polymeric Liquids: Fluid Mechanics* (John Wiley and Sons Inc., New York, 1987), Vol. 1.
 - [22] M. Goldin, J. Yerushalmi, R. Pfeffer, and R. Shinnar, Breakup of a laminar capillary jet of a viscoelastic fluid, *J. Fluid Mech.* **38**, 689 (1969).

- [23] D. W. Bousfield, R. Keunings, G. Marrucci, and M. M. Denn, Nonlinear analysis of the surface tension driven breakup of viscoelastic filaments, *J. Non-Newtonian Fluid Mech.* **21**, 79 (1986).
- [24] A. L. Yarin, *Free Liquid Jets and Films: Hydrodynamics and Rheology* (Longman Scientific & Technical, 1993).
- [25] H. J. Shore and G. M. Harrison, The effect of added polymers on the formation of drops ejected from a nozzle, *Phys. Fluids* **17**, 033104 (2005).
- [26] N. F. Morrison and O. G. Harlen, Viscoelasticity in inkjet printing, *Rheol. Acta* **49**, 619 (2010).
- [27] S. D. Hoath, D. C. Vadillo, O. G. Harlen, C. McIlroy, N. F. Morrison, W.-K. Hsiao, T. R. Tuladhar, S. Jung, G. D. Martin, and I. M. Hutchings, Inkjet printing of weakly elastic polymer solutions, *J. Non-Newtonian Fluid Mech.* **205**, 1 (2014).
- [28] Y. Amarouchene, D. Bonn, J. Meunier, and H. Kellay, Inhibition of the Finite-Time Singularity during Droplet Fission of a Polymeric Fluid, *Phys. Rev. Lett.* **86**, 3558 (2001).
- [29] S. L. Anna and G. H. McKinley, Elasto-capillary thinning and breakup of model elastic liquids, *J. Rheol.* **45**, 115 (2001).
- [30] C. Clasen, J. Eggers, M. A. Fontelos, J. Li, and G. H. McKinley, The beads-on-string structure of viscoelastic threads, *J. Fluid Mech.* **556**, 283 (2006).
- [31] P. P. Bhat, O. A. Basaran, and M. Pasquali, Dynamics of viscoelastic liquid filaments: Low capillary number flows, *J. Non-Newtonian Fluid Mech.* **150**, 211 (2008).
- [32] J. Eggers, M. A. Herrada, and J. Snoeijer, Self-similar breakup of polymeric threads as described by the Oldroyd-B model, *J. Fluid Mech.* **887**, A19 (2020).
- [33] J. Dinic, L. N. Jimenez, and V. Sharma, Pinch-off dynamics and dripping-onto-substrate (DoS) rheometry of complex fluids, *Lab Chip* **17**, 460 (2017).
- [34] J. Dinic and V. Sharma, Flexibility, extensibility, and ratio of Kuhn length to packing length govern the pinching dynamics, coil-stretch transition, and rheology of polymer solutions, *Macromolecules* **53**, 4821 (2020).
- [35] L. N. Jimenez, J. Dinic, N. Parsi, and V. Sharma, Extensional relaxation time, pinch-off dynamics, and printability of semidilute polyelectrolyte solutions, *Macromolecules* **51**, 5191 (2018).
- [36] G. I. Taylor, The dynamics of thin sheets of fluid. III. Disintegration of fluid sheets, *Proc. R. Soc. London* **253**, 313 (1959).
- [37] F. E. C. Culick, Comments on a ruptured soap film, *J. Appl. Phys.* **31**, 1128 (1960).
- [38] J.-L. Pierson, J. Magnaudet, E. J. Soares, and S. Popinet, Revisiting the Taylor-Culick approximation: Retraction of an axisymmetric filament, *Phys. Rev. Fluids* **5**, 073602 (2020).
- [39] X. Liu, B. W. Wagoner, H. Wee, and O. A. Basaran, Effect of initial conditions on promotion and inhibition of breakup during filament contraction, *AIChE J.* **68**, e17491 (2022).
- [40] M. A. Fontelos and J. Li, On the evolution and rupture of filaments in Giesekus and FENE models, *J. Non-Newtonian Fluid Mech.* **118**, 1 (2004).
- [41] M. Pasquali and L. Scriven, Free surface flows of polymer solutions with models based on the conformation tensor, *J. Non-Newtonian Fluid Mech.* **108**, 363 (2002).
- [42] C. R. Anthony, H. Wee, V. Garg, S. S. Thete, P. M. Kamat, B. W. Wagoner, E. D. Wilkes, P. K. Notz, A. U. Chen, R. Suryo, K. Sambath, J. C. Panditaratne, Y.-C. Liao, and O. A. Basaran, Sharp interface methods for simulation and analysis of free surface flows with singularities: Breakup and coalescence, *Annu. Rev. Fluid Mech.* **55**, 707 (2023).
- [43] J. Eggers, Universal Pinching of 3D Axisymmetric Free-Surface Flow, *Phys. Rev. Lett.* **71**, 3458 (1993).
- [44] J. Eggers and T. F. Dupont, Drop formation in a one-dimensional approximation of the Navier-Stokes equation, *J. Fluid Mech.* **262**, 205 (1994).
- [45] P. P. Bhat, S. Appathurai, M. T. Harris, and O. A. Basaran, On self-similarity in the drop-filament corner region formed during pinch-off of viscoelastic fluid threads, *Phys. Fluids* **24**, 083101 (2012).
- [46] B. Ambravaneswaran, S. D. Phillips, and O. A. Basaran, Theoretical Analysis of a Dripping Faucet, *Phys. Rev. Lett.* **85**, 5332 (2000).
- [47] B. Ambravaneswaran, E. D. Wilkes, and O. A. Basaran, Drop formation from a capillary tube: Comparison of one-dimensional and two-dimensional analyses and occurrence of satellite drops, *Phys. Fluids* **14**, 2606 (2002).

- [48] G. Debrégeas, P.-G. De Gennes, and F. Brochard-Wyart, The life and death of “Bare” viscous bubbles, *Science* **279**, 1704 (1998).
- [49] M. P. Brenner and D. Gueyffier, On the bursting of viscous films, *Phys. Fluids* **11**, 737 (1999).
- [50] N. Savva and J. W. Bush, Viscous sheet retraction, *J. Fluid Mech.* **626**, 211 (2009).
- [51] J. R. Castrejón-Pita, A. A. Castrejón-Pita, S. S. Thete, K. Sambath, I. M. Hutchings, J. Hinch, J. R. Lister, and O. A. Basaran, Plethora of transitions during breakup of liquid filaments, *Proc. Natl. Acad. Sci. USA* **112**, 4582 (2015).
- [52] P. M. Kamat, C. R. Anthony, and O. A. Basaran, Bubble coalescence in low-viscosity power-law fluids, *J. Fluid Mech.* **902**, A8 (2020).
- [53] P. K. Notz, A. U. Chen, and O. A. Basaran, Satellite drops: Unexpected dynamics and change of scaling during pinch-off, *Phys. Fluids* **13**, 549 (2001).
- [54] C. Planchette, F. Marangon, W.-K. Hsiao, and G. Brenn, Breakup of asymmetric liquid ligaments, *Phys. Rev. Fluids* **4**, 124004 (2019).

Correction: The year of publication in Ref. [42] was set incorrectly during the proof correction cycle and has been fixed.